Recent advances in Rydberg Physics using two-electron atoms

F. B. Dunning,[1] T.C. Killian,[1] S. Yoshida,[2] and J. Burgdörfer[2]

[1]*Department of Physics and Astronomy and the Rice Quantum Institute, Rice University, Houston, TX 77005-1892, USA*

[2]*Institute for Theoretical Physics, Vienna University of Technology, Vienna, Austria, EU*

Abstract

In this brief review, the opportunities that the alkaline-earth elements afford to study new aspects of Rydberg physics are discussed. For example, the bosonic alkaline-earth isotopes have zero nuclear spin which eliminates many of the complexities present in alkali Rydberg studies permitting simpler and more direct comparison between theory and experiment. The presence of two valence electrons allows the production of singlet and triplet Rydberg states that can exhibit a variety of attractive or repulsive interactions. The availability of weak intercombination lines is advantageous for laser cooling and for applications such as Rydberg dressing. Excitation of one electron to a Rydberg state leaves behind an optically-active core ion allowing, for high-L states, the optical imaging of Rydberg atoms and their (spatial) manipulation using light scattering. The second valence electron also opens up the possibility of engineering long-lived doubly-excited states such as planetary atoms. Recent advances in both theory and experiment are highlighted together with a number of possible directions for the future.

Rydberg atoms provide an excellent vehicle with which to study strongly-interacting quantum systems due to their long-range interactions. Such interactions can give rise to a number of interesting effects including dipole blockade in which multiple Rydberg excitations within some blockade sphere are inhibited due to the level shifts induced by the first Rydberg atom created. Dipole blockade can be exploited to entangle particles leading to creation of "superatoms" and for quantum gate operations and quantum state engineering [1–5]. Blockade also allows formation of highly-correlated many-body states [6] that can exhibit long-range crystalline order [7, 8] and can modify atom-light interactions giving rise to cooperative optical effects [8, 9]. Rydberg states permit the interactions between "ground-state" atoms to be continuously tuned by the introduction of a small admixture of Rydberg character into their wave functions through dressing with optical radiation tuned near resonance with the transition to the Rydberg state, the strength of the interactions being controlled by varying the size of the admixed fraction [10–14].

Many advances in Rydberg physics have been achieved using alkali Rydberg atoms. However, recently there has been increasing interest in the study of alkaline-earth Rydberg atoms which provide an opportunity to study new aspects of Rydberg physics. In particular, the presence of two valence electrons admits, within a single element, the production of both singlet and triplet states and of Rydberg states that can exhibit a variety of attractive or repulsive interactions. Furthermore, the availability of weak intercombination lines is advantageous for laser cooling such species and for applications such as Rydberg dressing [12, 13], generating spin-squeezed states [15], and atomic clocks. Furthermore, the presence of a pair of valence electrons leaves an optically active core ion after excitation of one of the electrons to a Rydberg state. For low-L states, excitation of the inner valence electron leads to autoionization which can be used to detect such states. For high-L states, the inner valence electron can be excited without inducing autoionization allowing the evolution of low-L states toward high-L states to be monitored as well as the optical imaging of the Rydberg atom and its (spatial) manipulation using light scattering. The second valence electron also admits the possibility of engineering long-lived doubly-excited states in the planetary atom or or frozen planet configurations [16–18]. Off resonance, optical transitions in the core ion can be used to create optical dipole traps for Rydberg atoms or magic wavelength optical potentials.

Initial studies of alkaline earth Rydberg atoms used a variety of elements including

barium, calcium, and strontium, and focused on the perturbation of Rydberg series introduced by interactions with neighboring doubly-excited states or an underlying continuum and, motivated by fundamental interest in the three-body Coulomb problem, on autoionization [19]. More recently, interest in alkaline-earth Rydberg atoms has expanded to include time-dependent studies of the dynamics of autoionization, high-resolution spectroscopy, measurements of quantum optical phenomena such as Autler-Townes splitting and electromagnetically-induced transparency (EIT), production of ultra-long-range Rydberg molecules, exploration of Rydberg dressing, and the creation of ultracold plasmas. Recognizing that it is impossible to review all the earlier work with alkaline-earth Rydberg atoms in a short article, we restrict discussion here to recent results obtained using (principally) strontium Rydberg atoms that illuminate opportunities for the future. However, other alkaline-earth and alkaline-earth-like species such as ytterbium can be used to explore much of the same physics.

I. EXPERIMENTAL CONSIDERATIONS

Strontium possesses four stable isotopes, three of which,^{84}Sr, ^{86}Sr, and ^{88}Sr, are bosonic and one, ^{87}Sr, fermionic. The most abundant isotope is ^{88}Sr (82.88%) followed by ^{86}Sr (9.86%), ^{87}Sr (7.00%), and ^{84}Sr (0.56%). We focus on the bosonic isotopes which have zero nuclear spin and hence no ground state hyperfine structure, greatly simplifying their excitation spectra. Beams of strontium atoms can be produced using an oven. However, the vapor pressure of strontium is significantly lower than that of the heavier alkali metals requiring the use of higher oven temperatures, $\sim$400-600 $^\circ$C, to achieve beam densities $\sim 10^9 \mathrm{cm}^{-3}$. Strontium Rydberg atoms can be detected using conventional techniques such as field ionization or ionization induced by collisions (Penning ionization) or by photoionization by background thermal radiation as well as by autoionization resulting from excitation of the core ion.

Figure 1 shows a partial term diagram for strontium that includes the atomic levels and transition wavelengths pertinent to the present discussion. Strontium singlet n^1S_0 and n^1D_2 Rydberg atoms can be conveniently created by two-photon excitation via the intermediate 5s5p $^1P_1$ state, radiation at the required wavelengths being readily generated using diode laser systems. Higher Rydberg production rates can be achieved by three-photon excitation

to n^1F_3 and n^1P_1 levels using the 5s5p ^{1}P$_1$ and 5s5d $^1D_2$ intermediate states because diode laser systems can provide high output powers (>1W) at 893 nm for the final excitation step. Two-photon excitation via the intermediate 5s5p $^3P_1$ state is used to generate n^3S_1 and $n^3D_{1,2,3}$ Rydberg states although the required radiation at 319 nm must be generated by second harmonic conversion.

Strontium is particularly amenable to laser cooling and trapping and all its isotopes have been cooled to quantum degeneracy [20]. Cooling generally proceeds in three steps. In the first step, atoms from a Zeeman slower are captured and cooled to milliKelvin temperatures at densities of $\sim 10^{10}$ cm^{-3} using a magneto-optical trap (MOT) operating on the broad "blue" 5s^2 $^1S_0$ - 5s5p $^1P_1$ transition at 461 nm. Atoms in the upper $^1P_1$ level, however, can decay via the $^1D_2$ level into the metastable 5s5p $^3P_2$ state, those metastable atoms in weak-field-seeking M_J states becoming trapped in the MOT magnetic field leading to the build up of a sizable population in this "reservoir" state. This population can be rapidly returned to the ground state by optical pumping into the shorter-lived ($\tau \sim 21$ μs) $^3P_1$ state via one of a number of intermediate states. The atoms can be recaptured and further cooled into the microKelvin regime using a "red" MOT operating on the $^1S_0$-$^3P_1$ transition at 689 nm, its narrow linewidth resulting in a much lower recoil-limited temperature than can be achieved in a "blue" MOT. Densities of $\sim 10^{12}$ cm^2 can be realized in a "red" MOT. These atoms can then be loaded into an optical dipole trap (ODT) and, once trapped therein, the "red" MOT can be turned off and evaporative cooling used to increase the phase space density and achieve temperatures of $\sim$100 nK and, ultimately, generate BECs. ^{84}Sr is especially well suited to evaporative cooling due to its moderate scattering length $a \sim 123$a$_0$, where a_0 is the Bohr radius. ^{86}Sr is also amenable to direct evaporative cooling although its larger scattering length, $\sim 800a_0$, requires use of large volume ODTs to obtain low atom densities to minimize three-body inelastic collision losses. ^{88}Sr is more challenging to cool due to its small negative scattering length $a \sim -2a_0$, which also results in collapse of the condensate above some critical atom number. Nonetheless, ^{88}Sr BECs have been produced in a "dimple" trap and by sympathetic cooling using ^{87}Sr as the refrigerant. ^{84}Sr atoms have been successfully loaded into optical lattices formed by three mutually orthogonal, retroreflected 532 nm laser beams.

II. THEORETICAL CONSIDERATIONS

The electronic structures of atoms are often described by several active electrons interacting with a model potential representing a mean interaction by a "frozen" configuration of the rest of electrons around the core ion. The alkalis are known to be well described by a single active electron model, i.e., a single electron moving in a model potential that incorporates the effect of core penetration by the valence electron. The situation for the alkaline earths is more complex as the excitation of a valence electron modifies the orbital of the rather weakly bound 2nd valence electron via electron-electron interaction. This leads to perturbation of the energy level structure due to the presence of doubly-excited perturber states. For barium there is a complex interplay between a large number of perturbers in many different series, thereby providing a major challenge to theory [21]. However, only a few perturber states ($5p^2$, $4d5p$, $4d^2$) are known for strontium around low-lying n levels. Therefore, the singly excited state $5snl$ for high n are not affected by the perturbers. For high n Rydberg states, the wave function near the core becomes independent of n due to strong Coulombic potential $-Z/r$ dominating over the bound energy $-1/(2n^2)$. The quantum defect theory [22] is based on this idea by representing the core interaction as a n-independent scattering phase shift (i.e. quantum defect) while the wavefunction outside the core region becomes a phase-shifted hydrogenic wavefunction (i.e. a superposition of regular and irregular Coulomb wave functions). Analogously, a single active electron model employing a n-independent (but ℓ-dependent) model potential including the influence of the 2nd valence electron [23] can be practical to describe such a core interaction. These calculations produce the wavefunctions outside the core region quite accurately. Therefore, the quantities such as the dipole transitions between high n Rydberg states are evaluated quite well.

These methods fail for low-lying n levels for which the electron-electron interaction becomes quite strong to mix the orbitals of the 2nd valence electron. For strontium indeed P and D states have relatively strong n-dependence in quantum defects confirming the mixing of orbitals. This can be overcome by employing the multichannel quantum defect theory (MQDT)[21, 22] in which eigenstates are a linear combination of several scattering channels. The admixture of regular and irregular wave functions in each channel and that of different channels have to be chosen to satisfy the boundary conditions of the wavefunction.

The parameters for the admixture are determined separately for each L-sector by fitting the results to measured data or, more rigorously, by employing the R-matrix theory in which the wavefunctions inside the core region are calculated using a model potential to determine the fitting parameters. Another venue to analyze the strontium electronic structure is a configuration interaction (CI) expansion of eigenstates using a two-active-electron (TAE) [24] model for which the Hamiltonian reads

$$H = \frac{p_1^2}{2} + \frac{p_2^2}{2} + V_{l_1}(r_1) + V_{l_2}(r_2) + \frac{1}{|\vec{r}_1 - \vec{r}_2|} \tag{1}$$

where $V_{l_i}(r_i)$ is an angular-momentum-dependent semi-empirical potential representing the Sr^{2+} core ion. (Unless otherwise noted atomic units are used throughout.) First, single particle orbitals $|\phi_{n_i}, l_i, m_i\rangle$ and orbital energies $E_{n_i l_i m_i}$ for the Sr^+ ion are generated with

$$H_{ion} = \frac{p^2}{2} + V_l(r) \tag{2}$$

These one-electron orbitals are used to construct basis states for the two-electron Hamiltonian that are symmetric(antisymmetric) with respect to exchange to represent singlet (triplet) states and the eigenfunctions and eigenenergies calculated by numerical diagonalization. For a accurate calculation of energy levels, the spin-orbit coupling

$$V_{LS}(r_1, r_2) = \frac{1}{2}\alpha^2 \vec{s}_1 \cdot \vec{\ell}_1 \frac{1}{r_1} V'(r_1) + \frac{1}{2}\alpha^2 \vec{s}_2 \cdot \vec{\ell}_2 \frac{1}{r_2} V'(r_2) \tag{3}$$

is added to evaluate the singlet-triplet mixing. For the study of single electron excitation the orbitals for the inner valence electron can be restricted to a few orbitals to reduce the size of calculations. This limitation in the number of configurations makes the CI-expansion analogous to the MQDT approach with R-matrix. For TAE calculations, once the parameters of the model potentials is fitted to measured spectra of Sr^+ ion, the eigenenergies of all L sectors can be calculated consistently. For Sr^+ ion, the measured data for p-states are limited allowing some error bar to fit the model potential. Otherwise the calculations show that excellent convergence in the spectra for the singly excited states is achieved using only six inner electron orbitals (5s, 4p, 5p, 6s, 5d, and 6p). The MQDT is a practical tool to analyze energy levels of multi-electron systems when the parameters to fit the measured data of the corresponding sector is known. The CI expansion requires a larger computing power. However, a numerical diagonalization of Hamiltonian typically yields the wavefunctions of the eigenstates. Therefore it is straight forward to evaluate their radial integrations to evaluate quantities, such as dipole matrix elements. This could be advantageous in particular for

high n states for which the integration of regular/irregular Coulomb wavefunctions becomes challenging. With both low- and high-n wavefunctions available the oscillator strengths from the ground state (or other low-n states) to highly excited Rydberg states become possible to study, for example, the blockade effect in photoexcitation of Rydberg atoms and the lifetime of Rydberg states.

III. SPECTROSCOPIC STUDIES

As noted earlier, initial spectroscopic studies of the alkaline-earths were designed to explore the perturbation of Rydberg series due to interactions with neighboring doubly-excited states or an underlying continuum, as well as investigate autoionization [19]. These studies provided the driver for many of the advances seen in MQDT. More recently spectroscopic measurements have been extended to cold ^{88}Sr gases allowing high resolution measurements [23]. The atoms were confined in a blue MOT equipped with a series of electrodes to allow application of controlled electric fields and accurate measurements of Stark spectra. The Rydberg atoms were created by two-photon excitation and were detected by measuring ions produced through Rydberg collisions or through autoionization. The presence of the Stark field allowed observation of otherwise forbidden transitions to $n^1\mathrm{P}_1$ states and the splitting of states into their component $|\mathrm{M}_J|$ levels. Figure 2 shows a Stark map recorded in the vicinity of the 5s80d $^1\mathrm{D}_2$ state. A number of singlet and triplet excited states are evident, each of which initially displays a quadratic Stark energy shift. Figure 2 also includes the results of detailed numerical calculations based on dipole matrix elements calculated using a SAE model and a potential derived using the known quantum defects. The calculated energy levels are in excellent quantitative agreement with the experimental data, especially for the singlet states, and the interaction with the Stark manifold of higher-L states is well described.

Spectroscopic studies of autoionization induced by excitation of the 408 nm 5s$n\ell$ $\rightarrow$5p$_{3/2}n'\ell$ transition in the core ion were also undertaken, the autoionization spectrum being measured by scanning the wavelength of the 408 nm laser [23, 25]. Representative autoionization spectra are shown in Fig. 3. The shapes and widths of the spectra depend strongly on the initial angular momentum ℓ of the Rydberg electron. The spectra were fit using a six-channel MQDT model. The excitation strength of autoionizing states can thus be

evaluated as the oscillator strength of the core electron excitation multiplied by the overlap of the outer electron wavefunctions between the bound and autoionizing states. Assuming that the inner valence electron is rather unaffected by the interaction with the outer electron (isolated core excitation), the excitation strength simply depends on the overlap of the outer electron wavefunctions, i.e., the difference $\epsilon = \delta_b$-δ_a between the quantum defect δ_b for the bound (Rydberg) state and that for the autoionizing state δ_a. For $\epsilon \simeq 0$ (modulo-one) each Rydberg state only overlaps with a single autoionizing state resulting in a single peak in the autoionizing spectra, as seen for the 20^1S_0 state for which $\epsilon = 0.15$. In contrast, for $\epsilon = 0.5$ (modulo-one) each Rydberg state overlaps with two autoionizing states and the autoionization spectrum becomes double-peaked as observed for the 19^1D_2 state for which $\epsilon = 0.46$. The widths of these (low-n) autoionization features are large, ~ 1 THz, and even for $n = 56$ remain >10 GHz indicating that autoionization is extremely rapid and can be used to probe the dynamics of cold Rydberg gases with high temporal resolution.

The dynamics of autoionization have been explored using coherent short-pulse laser excitation [26]. Spectrally-tailored picosecond laser pulses were employed to create radially-localized Rydberg wave packets (in barium). Such radial wave packets "breathe," their radial coordinates expanding and contracting as time increases. Two radial wave packets were excited sequentially each of which left the vicinity of the nucleus at a well-defined time. These radial wave packets subsequently "collided" as they passed through each other, the radius at which this collision occurred and thus the classical kinetic energy of the electrons at this time, being controlled by the time delay between their launches. Analysis of the data revealed that the energy transfer required to ionize the atom occurs in a single violent electron-electron collision rather than through a gradual exchange of energy between the electrons.

Spectroscopic measurements have been extended to very-high-n, $n \sim 500$, using a crossed laser-atom beam approach and an apparatus in which stray electric fields can be reduced to very low values, $\lesssim 50$ μV cm^{-1}, to prevent spurious perturbations of the high-n states [24, 27, 28]. In initial experiments two-photon excitation via the 5^1P_1 level was employed and the spectral resolution that could be achieved tested by measuring the isotope shifts in the high-n limit for the bosonic (strontium) isotopes. The spectra for each isotope were optimized by tuning the 461 nm laser to the specific wavelength required to excite $^1S_0$-$^1P_1$ transitions in that isotope. (Measurements with the ^{87}Sr isotope revealed strong hyperfine-

induced singlet-triplet mixing and strong interactions between states of different n.) Interest then shifted to the Stark spectrum and production of extreme red-shifted Stark states. Well-controlled excitation of such states in the presence of a dc electric field is key to production of strongly-polarized quasi-one-dimensional (quasi-1D) Rydberg atoms. Such atoms have large electric dipole moments and form the starting point for many of the techniques developed previously to control and manipulate high-n states using one, or more, carefully-tailored electric field pulses having characteristic times (duration, rise/fall times) $<T_n$, where T_n is the classical Kepler period ($\sim$4 ns at $n \sim 300$)[29–31]. While initially developed using alkali Rydberg atoms, these techniques can be equally well applied to strontium for which the high n states can be well described by a SAE model (i.e. the interaction with the 2nd valence electron in rather weak.) Two independent methods for probing the polarization of the Stark states were evaluated. In each approach short probe pulses were used to ionize the atoms and the resulting ionization (or survival) probabilities mapped to the polarization, i.e., the electric dipole moment [27]. As seen in Fig. 2, the low-L non-degenerate Stark states display, to leading order, a quadratic Stark effect and are, at least in modest applied fields, only weakly polarized. However, because L-mixing is weak, the oscillator strengths for their creation remain large. As the field is increased the isolated low-L states evolve onto quasi-hydrogenic states that display a near-linear Stark effect and can be strongly polarized. However, since they represent a superposition of many L states their low-L character is limited and, in consequence, their photoexcitation rates become small. This evolution towards quasi-1D states can be explored using a TAE model. Figure 4 shows the calculated scaled dipole moments $d = \langle z_1 + z_2 \rangle^2/n^2$ for the $|M_J| = 1$ states in the vicinity of $n = 50$ as a function of applied field, F_{dc}, scaled to the field, $F_{cross} = 1/(3n^5)$, around which states in neighboring manifolds first cross. The calculations indicated that in fields $F_{dc} \sim 0.8 F_{cross}$ "nD" states should possess dipole moments $\sim$1.0 to 1.2 n^2 au, a prediction confirmed experimentally in the high-n measurements. Application of the dc field, however, resulted in a marked decrease in the Rydberg atom production rate and attention therefore shifted to three-photon excitation of "nP" and "nF" states. Excitation in a field $F_{dc} \sim 0.3\ F_{cross}$ allowed production of ($n \sim$300) "nF" states with dipole moments of $\sim 1.2n^2$ and densities of $\sim 10^6$ cm^{-3}, even in a relatively low density ($\sim 10^9$ cm^{-3}) atomic beam.

In the absence of an electric field, n^1F_3 densities of $\sim$5x10^6 cm^{-3} were achieved corre-

sponding to interatomic spacings of $\sim$60 μm, below those required to study blockade effects in high-n atoms. A small excitation volume of $\sim 1.3\times10^{-7}$ cm^3 was defined using tightly-focused crossed laser beams. Measurement of the number and number distribution of n^1F_3 atoms created as a function of laser power and atom beam density revealed sizable blockade effects [32]. This is illustrated in Fig. 5 which shows the mean number $\langle \mathrm{N}_R \rangle$ of $n = 310$ Rydberg atoms created by a 130 ns-long laser pulse as a function of 893 nm laser power for several oven operating temperatures, i.e., beam densities. As $\langle \mathrm{N}_R \rangle$ increases, the Rydberg production rate deviates from the linear dependence expected in the absence of blockade effects and the number distribution becomes increasingly sub-Poissonian with Mandel Q parameters as large as -0.55. Blockade, however, is not complete which theory shows results because van der Waals interactions between n^1F_3 Rydberg atoms are anisotropic, their strengths depending on the relative orientations of the atoms. Nonetheless, the oscillator strength of the interacting pair become small as the target n^1F_3 pair coupled with other neighboring (optically inaccessible) pairs leading to suppression of excitation. Blockade both in beams and in cold gas samples promises creation of pairs of high-n Rydberg atoms with initially well-defined separations. If these atoms are initially well separated they should evolve essentially independently. Their mutual interactions might then be increased by using one, or more, electric field pulses to impulsively excite them to states of much higher n, the degree of coupling being tuned by varying the final target state (and interatomic spacing). Since the atoms are subject to the same pulse sequence, their initial electron motions are particularly well defined. The product two-electron wave packets therefore provide an opportunity to explore energy interchange and ionization in the time domain and search for long-lived configurations where, due to their correlated motions, the electrons remain far apart.

The availability of high-resolution spectroscopic data stimulated development of new MQDT models for the S, P, D, and F singlet and triplet Rydberg series in strontium using a reactance matrix approach [21]. These models provided results in excellent agreement with experimental data and were employed to analyze the Rydberg states considered in terms of channel fractions. Using these results the Landé g_J factors for the $^1\mathrm{D}_2$ and $^3\mathrm{D}_2$ series were calculated demonstrating the effect of singlet-triplet mixing in the D_2 states, together with the lifetimes of the $^1\mathrm{S}_0$ and $^1\mathrm{D}_2$ states where perturbers were found to lower their lifetimes significantly.

IV. ULTRA-LONG-RANGE RYDBERG MOLECULES

Scattering of the excited electron in a Rydberg atom from a neighboring ground state atom can bind the two atoms together to form an ultra-long-range Rydberg molecule with internuclear separations on the order of the size of the Rydberg atom, i.e., $\sim n^2$. Such molecules are of interest because they represent a new type of chemical bond and because they can display surprising features such as the presence of large permanent electric dipole moments, even in the case of a homonuclear molecule. The existence of ultra-long-range Rydberg molecules was originally predicted theoretically [33] but they have now been observed in a variety of species. Initial experiments involved spherically-symmetric Rb(nS) states [34, 35] and creation of molecules with small electric dipole moments but have now been extended to include anisotropic nP and nD states [36–41] and, using Cs(nS) states, to creation of so-called "trilobite" states that possess very large permanent electric dipole moments [42]. In addition, molecules comprising one Rydberg atom and up to four ground state atoms have been seen [43]. Detailed analysis of the data, however, is challenging due to the Rydberg electron spin-orbit and ground state hyperfine interactions which result in in the mixing of singlet and triplet electronic symmetries. For bosonic alkaline-earth atoms both these interactions are absent. Furthermore, electron scattering from ground-state rubidium and cesium atoms displays a strong p-wave shape resonance at low energies that further complicates the molecular structure and reduces the lifetime of Rydberg molecules (and Rydberg atoms) in a dense gas. Strontium, for which p-wave resonance at relatively high energy [44] does not play an important role for Rydberg molecule formation, therefore provides an attractive system for the study of Rydberg molecules as it allows straightforward direct comparison between theory and experiment [45]. The long lifetimes in a dense gas make strontium attractive for the study of Rydberg atoms as impurities in quantum systems [46]which, given the interest in the physics of charged particles immersed in quantum-degenerate gases, promises to be an active area of future research [47].

Figure 6 shows an excitation spectrum recorded using a cold sample of ^{84}Sr atoms with a peak density of $\sim$5x10^{13} cm^{-3} in the vicinity of the 5s38s ^{3}S$_1$ Rydberg state, the excited atoms/molecules being detected by field ionization. The features evident to the red of the parent Rydberg peak result from the production of Rydberg molecules. Figure 7 shows the results of calculations undertaken using a TAE model and first-order perturbation theory

that utilizes a Fermi pseudopotential and effective s- and p-wave scattering lengths to describe the interaction between the excited electron and ground state atom [45]. The resulting molecular potential is shown in Fig. 7 which also includes the calculated wave functions for the v=0, 1, and 2 vibrational levels. The v=0 wave function is strongly localized at large internuclear separations R in the outermost well of the molecular potential. The v=1 wave function extends over several wells and penetrates to somewhat smaller values of R. The v=2 wave function is even less well localized and extends to relatively small values of R. The calculated energy levels are included in Fig 6 and are in good agreement with the measured positions of the most prominent features as are the calculated relative excitation strengths.

The experimental results also show the presence of a number of smaller additional features that result from the creation of trimer states comprising a parent Rydberg atom and two bound atoms. The binding energies of such states are given approximately by the sum of the separate binding energies of the two atoms, which depends on their vibrational states. A feature associated with the production of a tetramer can also be identified in the figure.

An interesting question concerning Rydberg molecules relates to their lifetimes and how these compare to the lifetime of the parent Rydberg atom. Earlier studies using Rb(35s) parent atoms demonstrated that the lifetime of the parent atoms was significantly longer than that of the molecules, and that the lifetimes of the molecules themselves decreased with increasing vibrational excitation [48]. This behavior was attributed to the presence of the p-wave scattering resonance which results in a sharp decrease (step) in the molecular potential at relatively large internuclear separations. While this would suggest that the molecular constituents would move quickly to small internuclear separations where interactions might lead to rapid destruction, this is hindered by quantum reflection at the potential step resulting in reasonably long molecular lifetimes. As seen in Fig. 7 no such potential step is present at large internuclear separations for strontium, suggesting that, at least for the lower vibrational states, the lifetimes of the Rydberg molecules and parent atom should be equal which has now been confirmed experimentally. This observation highlights the relative simplicity of the interactions involved in the formation of strontium Rydberg molecules and points to their future use to test theories of molecular formation free of the complexities associated with the alkali Rydberg molecules.

V. RYDBERG DRESSING

As noted in the introduction, Rydberg dressing can be used to control the interaction between "ground state" atoms [12–14]. Theory predicts that such interactions can lead to a variety of interesting phenomena including creation of exotic spin and magnetic states [49, 50], three-dimensional solitons [51], and supersolids[10, 52, 53]. Studies of optical dressing of ^{84}Sr atoms contained in a cold gas or BEC have been undertaken using the dressing scheme shown in Fig. 8 which defines the relevant Rabi frequencies Ω_{01} and Ω_{12}, detunings δ_1, δ_2, and $\Delta = \delta_1 + \delta_2$, and the decay rates γ_1 and γ_2. For weak dressing (i.e., $\delta_1 \gg \Omega_{01}$ and $\Delta \gg \Omega_{eff}$ with an effective two-photon Rabi frequency $\Omega_{eff} = \Omega_{01}\Omega_{12}/(2|\delta_1|)$), the dressed atomic ground state becomes

$$|g'\rangle = \left(1 - \frac{\Omega_{01}^2}{8\delta_1^2} - \frac{\Omega_{eff}^2}{8\Delta^2}\right)|g\rangle + \frac{\Omega_{01}}{2\delta_1}|i\rangle + \frac{\Omega_{eff}}{2\Delta}|r\rangle \tag{4}$$

where $|g\rangle$, $|i\rangle$ and $|r\rangle$ denote the undressed ground, intermediate and Rydberg states respectively. Only for large intermediate state detunings, $\delta_1 \gg \Delta$, the intermediate state can be eliminated to reduce the system to a 2-level atom [54]. For typical densities of cold gases or BEC atom-atom interactions are sizable only among Rydberg atoms independent of the population in the $|g\rangle$ or $|i\rangle$ state. Thus the interaction strength, which vary as $\Omega_{eff}^2/4\Delta^2$ can then be manipulated by varying Ω_{eff} and Δ. Strontium atoms are attractive for studies involving Rydberg dressing because, when compared to alkali atoms, two-photon excitation to triplet Rydberg levels via the long-lived triplet intermediate state can reduce decoherence from light scattering for a given level of Rydberg coupling.

Measurements on ^{84}Sr cold-gas samples and BECs held in an ODT and dressed with the 30^3S_1 state, however, have demonstrated that even weak dressing can lead to surprisingly large atom loss rates from the trap. The processes responsible were examined through a series of density- and time-dependent measurements. One such measurement is illustrated in Fig. 9 which shows the measured decrease in the number of ground state atoms present in the trap for a BEC containing $\sim 5\times10^5$ atoms at a density of $\sim 5\times10^{13}$ cm^{-3} and a temperature of 30 nK as a function of overall detuning Δ for several different dressing times, t_{on}. The width of the trap loss feature increases as the dressing time is increased and for a dressing time of 250 μs large trap losses are seen even when well detuned from resonance. Indeed, at a detuning $\Delta/2\pi \sim$ 11 MHz, i.e., for $\Omega_{eff}^2/2\Delta^2 \sim 5\times10^{-6}$, some 25% of

the atoms initially present are lost. The measurements suggest that ground state atom loss is associated with the excitation of Rydberg atoms which can result in direct atom loss through recoil and in the population of the very-long-lived 5s5p $^3P_0$ and $^3P_2$ metastable state. At large detunings the Rydberg population $\sim \Omega_{eff}^2/4\Delta^2$ and the rate of the following decay to long-lived states $\sim \Omega_{eff}^2\ \gamma_2/4\Delta^2$ are small and cannot account for the observed losses. Other potential loss mechanisms are therefore under consideration. One possibility is the enhanced Rydberg excitation induced by dephasing (decoherence) [55] through which dressed states stochastically collapse to one of undressed states. Once one, or a few, atoms collapse to the Rydberg state, it might trigger excitation of further atoms resulting in a "near-avalanche-like" growth in the Rydberg population [56, 57]. Such a process leads to a power-law growth suggesting a sizable time delay before significant trap loss becomes observable (see the inset in Fig. 9). At the high atom densities found in cold atom samples the nearest neighbor separations are much less than the blockade radius whereupon Rydberg-Rydberg interactions can lead to sizable energy shifts. In the case of n $^3S_1$ states which display strong, isotropic, short-range repulsive interactions this allows resonant Rydberg excitation when blue detuned but cannot account for the loss seen when red detuned. While charged particle production might lead to Stark shifts and line broadening, application of an electric field to remove any ions present resulted in no significant change in the results. Many of the experimental observations can be explained by rapid dephasing or decoherence of the dressed state. One of the possible origins for dephasing/decoherence is the interaction of the cold gas with the ambient photon bath. Due to blackbody-radiation-induced transitions and their enhancement by superradiance atoms in nearby ^3P states are populated. Their dipole-dipole interactions with $^3S_1$ atoms could be another trigger for a avalanche-like growth. Experiments with dressed alkali atoms have also revealed unexpectedly large interaction-induced broadening [58–60] which was explained in terms of dipole-dipole interactions with neighboring P states [60].

Trap losses severely limit both the strength of the dressing that can be applied and for how long. Nevertheless, the effects of dressing have been observed in systems with many fewer atoms. These results, and those described above in larger systems suggest that, if effects due to dressing are to be observed, small samples and\or short time scales may be essential.

VI. RYDBERG-RYDBERG INTERACTIONS

As noted above, the generation of controlled unitary interactions in large ensembles through Rydberg dressing is challenging because of the large loss and dephasing rates seen experimentally and the many open questions concerning the mechanisms responsible. The correct description of the correlations induced by Rydberg blockade and Rydberg dressing in dense gases is an active area of study and has been addressed by two-photon excitation of alkali atoms in a three-level ladder configuration where, depending as to the relative excitation strengths of the two lasers employed, three different regimes can be accessed corresponding to coherent population trapping (CPT) [61, 62], electromagnetically-induced transparency (EIT) [9, 62], and Autler-Townes (AT) spectroscopy [63]. For the alkalis typically the laser coupling between the ground and the intermediate states is much stronger than that between the intermediate and the Rydberg states yielding a laser dressed state as a superposition of the ground and the intermediate states. In contrast, when working with the triplet states of strontium, the intermediate state is very weakly coupled to the ground state and the dressed states, superpositions of the intermediate and the Rydberg states, are probed by a weak probe laser coupled to the ground state. Therefore, Rydberg state decay provides the dominant source of decoherence against the dressed states enabling AT spectroscopy of strongly-driven Rydberg systems under conditions where the Rydberg population is small.

Figure 10 shows the results of dressing a sample of ^{84}Sr atoms with a peak density of $\sim 1\times10^{13}$ cm^{-3} held in an ODT with the 5s24s ^{3}S$_1$ Rydberg state via the intermediate ^{3}P$_1$ state (see Fig. 8) [64]. (The lifetime of the 24 ^{3}S$_1$ state, $\tau(^3\mathrm{S}_1) \sim 4$ μs, is significantly smaller than that of the 5^{3}P$_1$ state, ~ 21 μs.) The 319 nm laser is tuned on resonance, $\delta_{12} = 0$ and provides a Rabi frequency $\Omega_{12}/2\pi = 2.4$ MHz. The 689 nm laser is scanned between detuning limits $\delta_{01}/2\pi$ of ± 2 MHz, with the Rabi frequency Ω_0, set to the values indicated and is chopped to provide output pulses of 2μs duration. Figure 10 shows the fraction of ground state atoms remaining in the trap after one such pulse as a function of the detuning of the 689 nm laser for the Rabi frequencies Ω_{01} indicated. For the smallest value of Ω_{01} an almost symmetrical AT spectrum is observed, typical of a non-interacting gas. As Ω_{01} is increased shifts and asymmetries appear in the spectra pointing to increased interactions. To explain this behavior a density matrix model was developed based on a one-body description but including non-linear energy shifts and dephasing rates that depend on the Rydberg density.

The model incorporates a mean field energy shift that accounts for the short-range cut-off in Rydberg-Rydberg separations set by the blockade radius for the van der Waals interaction. The model results presented in Fig. 10 assume that the nonlinear shift and dephasing rate are of equal magnitude. The reasonable agreement with the experimental data, especially for the lower values of Ω_{01}, highlights the important role played by blockade effects. As Ω_{01} is increased, clear signatures of increased dephasing appear through the broadening of the lines and increased atom loss on center line. To explore this, measurements were undertaken for longer excitation times, and data recorded for an exposure time of $\sim$7 μs with $\Omega_{01}/2\pi$ = 133 kHz are included in Fig. 10

The atom loss spectrum is changed dramatically, collapsing to a single peak near line center. This total loss of coherence of the dressed state implies dephasing on a time scale that is much faster than the Rabi frequency Ω_{12} and much larger than the dephasing rates that reproduced the spectra seen for short exposure times. Nonetheless, related work has shown that two-photon resonant optical pumping to Rydberg states can lead to enhanced effective interactions and provide increased coherence times. The possibility of engineering atomic interactions under Rydberg EIT conditions opens up new opportunities to probe the coupled non-linear dynamics of light and matter wave fields. This work also further demonstrates that the availability of a narrow-linewidth intermediate state in the alkaline earths is critical for obtaining longer coherence times.

VII. ULTRACOLD NEUTRAL PLASMAS

Excitation of a cold gas to Rydberg states can lead to collisions and Penning ionization, triggering a collisional cascade that can spontaneously transform a Rydberg gas into an ultracold neutral plasma [65–67]. Most earlier experimental studies of such evolution utilized laser cooled alkali or alkali-like atoms including rubidium, cesium, and metastable xenon. The principal diagnostic employed to monitor such evolution was the detection of charged particles that escaped the plasma or that were stripped from the atoms (or plasma) by an applied field. However, while selective field ionization (SFI) provides a measure of state selectivity, it provides no spatial resolution unless, for example, used with highly-magnifying charged particle optics [68]. For the alkaline-earths, however, the scattering of resonant light off the core ions can provide spatially and temporally resolved *in situ* imaging. Such laser-

induced fluorescence (LIF) provides a valuable tool with which to follow the evolution and collisional dynamics of Rydberg populations.

The power of this technique has been demonstrated using ^{88}Sr atoms initially held in a "blue" MOT and excited to either the 5s48s $^1S_0$ or 5s47d $^1D_2$ state [69]. The core ions were imaged using the $5s^2S_{1/2}$-$5p^2P_{1/2}$ transition at 422 nm. Figure 11 shows the spontaneous evolution of the number of visible core ions as a function of time following excitation $\sim 10^6$ $^1S_0$ or $^1D_2$ Rydberg atoms in a "cigar-shaped" cloud with dimensions of $\sim 1 \times 3$ mm. These images provide a sensitive spatially-resolved probe of the collision dynamics, i.e., whether or not the parent Rydberg atoms remain in their initial low-L states for which core ion excitation would lead to autoionzation rather than to fluorescence. Transitions to high-L states induced by "ℓ-changing" in Rydberg-Rydberg collisions, or in collisions with low-energy electrons liberated through Penning ionization renders the core ions visible, as does Penning ionization or electron impact ionization. As seen in Fig. 11, while the general characteristics of the evolution of the $^1S_0$ and $^1D_2$ clouds are similar, i.e., visibility starts in the densest regions and propagates in space and time to encompass the entire cloud, the time scale for this evolution is noticeably slower for the $^1D_2$ cloud, the growth in the number of visible ion cores being significantly less rapid than for the $^1S_0$ states. This is explained by noting that interactions between the $^1S_0$ states are attractive whereas those between $^1D_2$ states are largely repulsive.

As illustrated in Fig. 11, core ion imaging allows detailed study of the dynamics governing the evolution of an ultracold gas of Rydberg atoms, in particular of the ℓ-changing collisions that occur during the early stages of the evolution. Furthermore, it was shown that the introduction of low-energy "seed" photoelectrons leads to rapid ionization providing a means to determine the total number and density of Rydberg atoms present at the time of their introduction. LIF can provide high time resolution, $\sim$10 ns, and as seen in Fig. 11, spatial resolutions of $\sim$200 μm are readily achievable, although this could be significantly improved by use of better optics. LIF should be particularly valuable for imaging spatial correlations such as might arise from dipole blockade in a one- or two-dimensional ODT. Dipole blockade has been proposed as a way to create even colder ultracold neutral plasmas as it allows excitation of an ordered array of Rydberg atoms which can then be ionized using "seed" electrons resulting in the production of an ordered array of core ions which would greatly reduce subsequent disorder-induced heating. The plasma temperature might also be reduced

by laser cooling the core ions using the $5s(^2S_{1/2})\rightarrow 5p(^2P_{1/2,3/2})$ transitions. Divalent atoms also allow for relatively straightforward ionization of singly charged ions. This has been studied with calcium as a possible way to form more strongly interacting ultracold plasmas [70].

VIII. SUMMARY

Interest in the alkaline-earth atoms has increased rapidly in recent years because they provide the opportunity to study many aspects of Rydberg physics related to, for example, two-electron excited states, the properties of ultralong-range Rydberg molecules, and Rydberg dressing and the control of few- and many-body interacting systems. Recent advances have exploited some, but by no means all, of these opportunities and this, coupled with the many questions this work has raised, suggest that interest in the alkaline-earths will only continue to grow in the future.

Acknowledgments

It is a pleasure to acknowledge the help of X. Zhang, J. A. Aman, and F. Camargo in the preparation of figures for this article. The research by the authors and their colleagues described here was supported by the NSF under grants Nos. 1301773 and 1205946, by the AFOSR under grant No. FA9550-12-1-0267, by the Robert A. Welch Foundation under grants Nos. C-0734 and C-1844, and by the FWF (Austria) under grant No. P23359-N16 and by the SFB-NextLite.

[1] M. D. Lukin, M. Fleischhauer, R. Cote, L. M. Duan, D. Jaksch, J. I. Cirac, and P. Zoller, Phys. Rev. Lett. **87**, 037901 (2001), URL http://link.aps.org/doi/10.1103/PhysRevLett.87.037901.

[2] E. Urban, T. A. Johnson, T. Henage, L. Isenhower, D. D. Yavuz, T. G. Walker, and M. Saffman, Nature Physics **5**, 110 (2009), ISSN 17452473, URL http://search.ebscohost.com.ezproxy.rice.edu/login.aspx?direct=true&db=a9h&AN=36336650&site=ehost-live&scope=site.

[3] A. Gatan, Y. Miroshnychenko, T. Wilk, A. Chotia, M. Viteau, D. Comparat, P. Pillet, A. Browaeys, and P. Grangier, Nature Physics **5**, 115 (2009), ISSN 17452473, URL http://search.ebscohost.com.ezproxy.rice.edu/login.aspx?direct=true&db=a9h&AN=36336649&site=ehost-live&scope=site.

[4] R. Heidemann, U. Raitzsch, V. Bendkowsky, B. Butscher, R. Löw, L. Santos, and T. Pfau, Phys. Rev. Lett. **99**, 163601 (2007), URL http://link.aps.org/doi/10.1103/PhysRevLett.99.163601.

[5] M. Saffman, T. G. Walker, and K. Mølmer, Rev. Mod. Phys. **82**, 2313 (2010), URL http://link.aps.org/doi/10.1103/RevModPhys.82.2313.

[6] H. Weimer, R. Löw, T. Pfau, and H. P. Büchler, Phys. Rev. Lett. **101**, 250601 (2008), URL http://link.aps.org/doi/10.1103/PhysRevLett.101.250601.

[7] T. Pohl, E. Demler, and M. D. Lukin, Phys. Rev. Lett. **104**, 043002 (2010), URL http://link.aps.org/doi/10.1103/PhysRevLett.104.043002.

[8] J. Schachenmayer, I. Lesanovsky, A. Micheli, and A. J. Daley, New Journal of Physics **12**, 103044 (2010), URL http://stacks.iop.org/1367-2630/12/i=10/a=103044.

[9] J. D. Pritchard, D. Maxwell, A. Gauguet, K. J. Weatherill, M. P. A. Jones, and C. S. Adams, Phys. Rev. Lett. **105**, 193603 (2010), URL http://link.aps.org/doi/10.1103/PhysRevLett.105.193603.

[10] N. Henkel, R. Nath, and T. Pohl, Phys. Rev. Lett. **104**, 195302 (2010), URL http://link.aps.org/doi/10.1103/PhysRevLett.104.195302.

[11] J. Honer, H. Weimer, T. Pfau, and H. P. Büchler, Phys. Rev. Lett. **105**, 160404 (2010), URL http://link.aps.org/doi/10.1103/PhysRevLett.105.160404.

[12] J. E. Johnson and S. L. Rolston, Phys. Rev. A **82**, 033412 (2010), URL http://link.aps.org/doi/10.1103/PhysRevA.82.033412.

[13] J. B. Balewski, A. T. Krupp, A. Gaj, S. Hofferberth, R. L??w, and T. Pfau, New Journal of Physics **16**, 063012 (2014), URL http://stacks.iop.org/1367-2630/16/i=6/a=063012.

[14] Y.-Y. Jau, A. M. Hankin, T. Keating, I. H. Deutsch, and G. W. Biedermann, ArXiv e-prints (2015), 1501.03862.

[15] L. I. R. Gil, R. Mukherjee, E. M. Bridge, M. P. A. Jones, and T. Pohl, Phys. Rev. Lett. **112**, 103601 (2014), URL http://link.aps.org/doi/10.1103/PhysRevLett.112.103601.

[16] I. C. Percival, Proceedings of the Royal Society of London A: Mathematical, Physical and Engineering Sciences **353**, 289 (1977), ISSN 0080-4630.

[17] G. Tanner, K. Richter, and J.-M. Rost, Rev. Mod. Phys. **72**, 497 (2000), URL http://link.aps.org/doi/10.1103/RevModPhys.72.497.

[18] M. Kalinski, J. H. Eberly, J. A. West, and C. R. Stroud, Phys. Rev. A **67**, 032503 (2003), URL http://link.aps.org/doi/10.1103/PhysRevA.67.032503.

[19] T. F. Gallagher, *Rydberg Atoms* (Cambridge University Press, 1994).

[20] S. Stellmer, F. Schreck, and T. Killian, *Annual Review of Cold Atoms and Molecules*, vol. 2 (World Scientific, Singapore, 2014).

[21] C. L. Vaillant, M. P. A. Jones, and R. M. Potvliege, Journal of Physics B: Atomic, Molecular and Optical Physics **47**, 155001 (2014), URL http://stacks.iop.org/0953-4075/47/i=15/a=155001.

[22] M. J. Seaton, Reports on Progress in Physics **46**, 167 (1983), URL http://stacks.iop.org/0034-4885/46/i=2/a=002.

[23] J. Millen, G. Lochead, G. R. Corbett, R. M. Potvliege, and M. P. A. Jones, Journal of Physics B: Atomic, Molecular and Optical Physics **44**, 184001 (2011), URL http://stacks.iop.org/0953-4075/44/i=18/a=184001.

[24] S. Ye, X. Zhang, T. C. Killian, F. B. Dunning, M. Hiller, S. Yoshida, S. Nagele, and J. Burgdörfer, Phys. Rev. A **88**, 043430 (2013), URL http://link.aps.org/doi/10.1103/PhysRevA.88.043430.

[25] J. Millen, G. Lochead, and M. P. A. Jones, Phys. Rev. Lett. **105**, 213004 (2010), URL http://link.aps.org/doi/10.1103/PhysRevLett.105.213004.

[26] S. N. Pisharody and R. R. Jones, Science **303**, 813 (2004), ISSN 00368075, URL

http://search.ebscohost.com.ezproxy.rice.edu/login.aspx?direct=true&db=a9h&AN=12306167&site=ehost-live&scope=site.

[27] M. Hiller, S. Yoshida, J. Burgdörfer, S. Ye, X. Zhang, and F. B. Dunning, Phys. Rev. A **89**, 023426 (2014), URL http://link.aps.org/doi/10.1103/PhysRevA.89.023426.

[28] S. Ye, X. Zhang, F. B. Dunning, S. Yoshida, M. Hiller, and J. Burgdörfer, Phys. Rev. A **90**, 013401 (2014), URL http://link.aps.org/doi/10.1103/PhysRevA.90.013401.

[29] F. B. Dunning, J. J. Mestayer, C. O. Reinhold, S. Yoshida, and J. Burgd??rfer, Journal of Physics B: Atomic, Molecular and Optical Physics **42**, 022001 (2009), URL http://stacks.iop.org/0953-4075/42/i=2/a=022001.

[30] F. B. Dunning, C. O. Reinhold, S. Yoshida, and J. Burgdörfer, American Journal of Physics **133**, 064301 (2010).

[31] B. Wyker, S. Ye, F. B. Dunning, S. Yoshida, C. O. Reinhold, and J. Burgdörfer, Phys. Rev. Lett. **108**, 043001 (2012), URL http://link.aps.org/doi/10.1103/PhysRevLett.108.043001.

[32] (????).

[33] C. H. Greene, A. S. Dickinson, and H. R. Sadeghpour, Phys. Rev. Lett. **85**, 2458 (2000), URL http://link.aps.org/doi/10.1103/PhysRevLett.85.2458.

[34] V. Bendkowsky, B. Butscher, J. Nipper, J. P. Shaffer, R. Lw, and T. Pfau, Nature **458**, 1005 (2009), ISSN 00280836, URL http://search.ebscohost.com.ezproxy.rice.edu/login.aspx?direct=true&db=a9h&AN=38219469&site=ehost-live&scope=site.

[35] W. Li, T. Pohl, J. M. Rost, S. T. Rittenhouse, H. R. Sadeghpour, J. Nipper, B. Butscher, J. B. Balewski, V. Bendkowsky, R. Low, et al., Science **334**, 1110 (2011), ISSN 00368075, URL http://search.ebscohost.com.ezproxy.rice.edu/login.aspx?direct=true&db=a9h&AN=67764706&site=ehost-live&scope=site.

[36] J. Tallant, S. T. Rittenhouse, D. Booth, H. R. Sadeghpour, and J. P. Shaffer, Phys. Rev. Lett. **109**, 173202 (2012), URL http://link.aps.org/doi/10.1103/PhysRevLett.109.173202.

[37] M. A. Bellos, R. Carollo, J. Banerjee, E. E. Eyler, P. L. Gould, and W. C. Stwalley, Phys. Rev. Lett. **111**, 053001 (2013), URL http://link.aps.org/doi/10.1103/PhysRevLett.111.053001.

[38] D. A. Anderson, S. A. Miller, and G. Raithel, Phys. Rev. Lett. **112**, 163201 (2014), URL http://link.aps.org/doi/10.1103/PhysRevLett.112.163201.

[39] A. T. Krupp, A. Gaj, J. B. Balewski, P. Ilzhöfer, S. Hofferberth, R. Löw, T. Pfau, M. Kurz, and P. Schmelcher, Phys. Rev. Lett. **112**, 143008 (2014), URL http://link.aps.org/doi/10.1103/PhysRevLett.112.143008.

[40] H. Saßmannshausen, F. Merkt, and J. Deiglmayr, Phys. Rev. Lett. **114**, 133201 (2015), URL http://link.aps.org/doi/10.1103/PhysRevLett.114.133201.

[41] A. Gaj, A. T. Krupp, P. Ilzhöfer, R. Löw, S. Hofferberth, and T. Pfau, Phys. Rev. Lett. **115**, 023001 (2015), URL http://link.aps.org/doi/10.1103/PhysRevLett.115.023001.

[42] D. Booth, S. T. Rittenhouse, J. Yang, H. R. Sadeghpour, and J. P. Shaffer, Science **348**, 99 (2015), ISSN 00368075, URL http://search.ebscohost.com.ezproxy.rice.edu/login.aspx?direct=true&db=a9h&AN=101903702&site=ehost-live&scope=site.

[43] A. Gaj, A. T. Krupp, J. B. Balewski, R. Löw, S. Hofferberth, and T. Pfau, Nature communications **5** (2014).

[44] J. Yuan and Z. Zhang, Phys. Rev. A **42**, 5363 (1990), URL http://link.aps.org/doi/10.1103/PhysRevA.42.5363.

[45] B. J. DeSalvo, J. A. Aman, F. B. Dunning, T. C. Killian, H. R. Sadeghpour, S. Yoshida, and J. Burgdörfer, Phys. Rev. A **92**, 031403 (2015), URL http://link.aps.org/doi/10.1103/PhysRevA.92.031403.

[46] J. B. Balewski, A. T. Krupp, A. Gaj, D. Peter, H. P. Bchler, R. Lw, S. Hofferberth, and T. Pfau, Nature **502**, 664 (2013), ISSN 00280836, URL http://search.ebscohost.com.ezproxy.rice.edu/login.aspx?direct=true&db=a9h&AN=91734603&site=ehost-live&scope=site.

[47] T. Karpiuk, M. Brewczyk, K. Rz??ewski, A. Gaj, J. B. Balewski, A. T. Krupp, M. Schlagm?ller, R. L??w, S. Hofferberth, and T. Pfau, New Journal of Physics **17**, 053046 (2015), URL http://stacks.iop.org/1367-2630/17/i=5/a=053046.

[48] B. Butscher, V. Bendkowsky, J. Nipper, J. B. Balewski, L. Kukota, R. L??w, T. Pfau, W. Li, T. Pohl, and J. M. Rost, Journal of Physics B: Atomic, Molecular and Optical Physics **44**, 184004 (2011), URL http://stacks.iop.org/0953-4075/44/i=18/a=184004.

[49] A. W. Glaetzle, M. Dalmonte, R. Nath, C. Gross, I. Bloch, and P. Zoller, Phys. Rev. Lett. **114**, 173002 (2015), URL http://link.aps.org/doi/10.1103/PhysRevLett.114.173002.

[50] R. M. W. van Bijnen and T. Pohl, Phys. Rev. Lett. **114**, 243002 (2015), URL http://link.aps.org/doi/10.1103/PhysRevLett.114.243002.

[51] F. Maucher, N. Henkel, M. Saffman, W. Królikowski, S. Skupin, and T. Pohl, Phys. Rev. Lett. **106**, 170401 (2011), URL http://link.aps.org/doi/10.1103/PhysRevLett.106.170401.

[52] G. Pupillo, A. Micheli, M. Boninsegni, I. Lesanovsky, and P. Zoller, Phys. Rev. Lett. **104**, 223002 (2010), URL http://link.aps.org/doi/10.1103/PhysRevLett.104.223002.

[53] M. Boninsegni and N. V. Prokof'ev, Rev. Mod. Phys. **84**, 759 (2012), URL http://link.aps.org/doi/10.1103/RevModPhys.84.759.

[54] T. R. Gentile, B. J. Hughey, D. Kleppner, and T. W. Ducas, Phys. Rev. A **40**, 5103 (1989), URL http://link.aps.org/doi/10.1103/PhysRevA.40.5103.

[55] D. W. Schönleber, M. Gärttner, and J. Evers, Phys. Rev. A **89**, 033421 (2014), URL http://link.aps.org/doi/10.1103/PhysRevA.89.033421.

[56] H. Schempp, G. Günter, M. Robert-de Saint-Vincent, C. S. Hofmann, D. Breyel, A. Komnik, D. W. Schönleber, M. Gärttner, J. Evers, S. Whitlock, et al., Phys. Rev. Lett. **112**, 013002 (2014), URL http://link.aps.org/doi/10.1103/PhysRevLett.112.013002.

[57] N. Malossi, M. M. Valado, S. Scotto, O. Morsch, E. Arimondo, and D. Ciampini, Journal of Physics: Conference Series **497**, 012031 (2014), URL http://stacks.iop.org/1742-6596/497/i=1/a=012031.

[58] T. Wang, S. F. Yelin, R. Côté, E. E. Eyler, S. M. Farooqi, P. L. Gould, M. Koštrun, D. Tong, and D. Vrinceanu, Phys. Rev. A **75**, 033802 (2007), URL http://link.aps.org/doi/10.1103/PhysRevA.75.033802.

[59] K. J. Weatherill, J. D. Pritchard, R. P. Abel, M. G. Bason, A. K. Mohapatra, and C. S. Adams, Journal of Physics B: Atomic, Molecular and Optical Physics **41**, 201002 (2008), URL http://stacks.iop.org/0953-4075/41/i=20/a=201002.

[60] E. A. Goldschmidt, T. Boulier, R. C. Brown, S. B. Koller, J. T. Young, A. V. Gorshkov, S. L. Rolston, and J. V. Porto, ArXiv e-prints (2015), 1510.08710.

[61] H. Schempp, G. Günter, C. S. Hofmann, C. Giese, S. D. Saliba, B. D. DePaola, T. Amthor, M. Weidemüller, S. Sevinli, and T. Pohl, Phys. Rev. Lett. **104**, 173602 (2010), URL http://link.aps.org/doi/10.1103/PhysRevLett.104.173602.

[62] S. Sevin?li, C. Ates, T. Pohl, H. Schempp, C. S. Hofmann, G. G?nter, T. Amthor, M. Weidem?ller, J. D. Pritchard, D. Maxwell, et al., Journal of Physics B: Atomic, Molecular and Optical Physics **44**, 184018 (2011), URL http://stacks.iop.org/0953-4075/44/i=18/a=184018.

[63] H. Zhang, L. Zhang, L. Wang, S. Bao, J. Zhao, S. Jia, and G. Raithel, Phys. Rev. A **90**, 043849 (2014), URL http://link.aps.org/doi/10.1103/PhysRevA.90.043849.

[64] B. J. DeSalvo, J. A. Aman, C. Gaul, T. Pohl, S. Yoshida, J. Burgdörfer, K. R. A. Hazzard, F. B. Dunning, and T. C. Killian, ArXiv e-prints (2015), 1510.08032.

[65] M. P. Robinson, B. L. Tolra, M. W. Noel, T. F. Gallagher, and P. Pillet, Phys. Rev. Lett. **85**, 4466 (2000), URL http://link.aps.org/doi/10.1103/PhysRevLett.85.4466.

[66] F. Robicheaux, Journal of Physics B: Atomic, Molecular and Optical Physics **38**, S333 (2005), URL http://stacks.iop.org/0953-4075/38/i=2/a=024.

[67] T. C. Killian, T. Pattard, T. Pohl, and J. M. Rost, Physics Reports **449**, 77 (2007).

[68] A. Schwarzkopf, R. E. Sapiro, and G. Raithel, Phys. Rev. Lett. **107**, 103001 (2011), URL http://link.aps.org/doi/10.1103/PhysRevLett.107.103001.

[69] P. McQuillen, X. Zhang, T. Strickler, F. B. Dunning, and T. C. Killian, Phys. Rev. A **87**, 013407 (2013), URL http://link.aps.org/doi/10.1103/PhysRevA.87.013407.

[70] M. Lyon, S. D. Bergeson, A. Diaw, and M. S. Murillo, Phys. Rev. E **91**, 033101 (2015), URL http://link.aps.org/doi/10.1103/PhysRevE.91.033101.

Figures

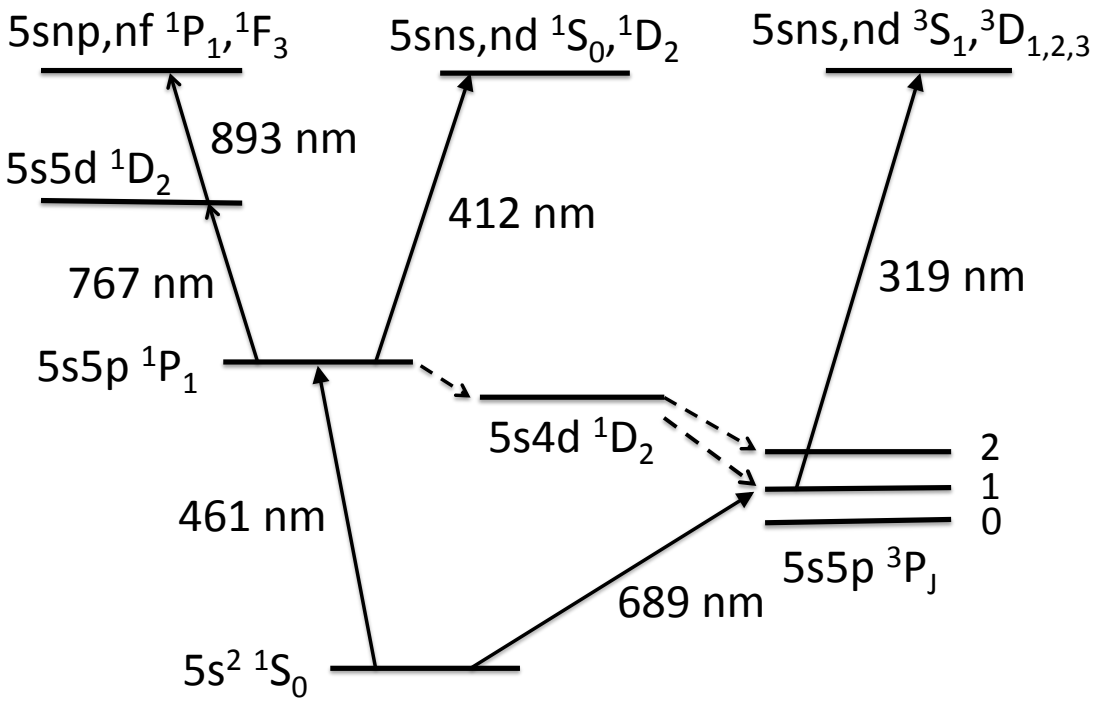

FIG. 1: Partial strontium term diagram showing the transitions of interest in production of singlet and triplet Rydberg states.

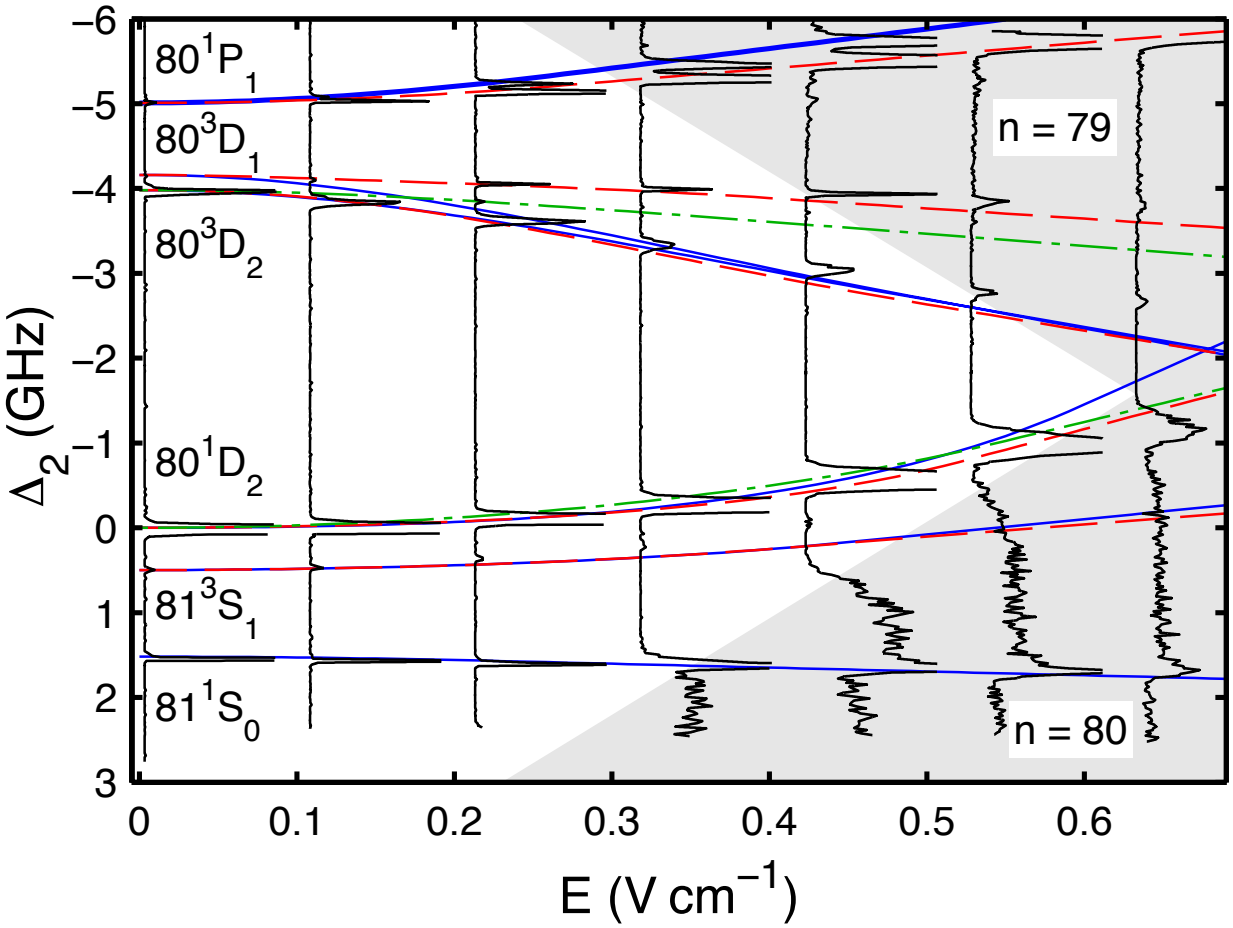

FIG. 2: Stark spectrum for strontium in the vicinity of the 5s80d $^1D_2$ state. The solid black lines are experimental data recorded as a function of detuning Δ_2 from the zero-field 80^1D_2 state. The blue (solid), red (dashed), and green (dot-dashed) lines show calculated $|M_J|$=0, 1, and 2 levels, respectively. The shaded areas delineate the boundaries of the manifold of high-angular-momentum Stark states. (Taken from ref.[?].)

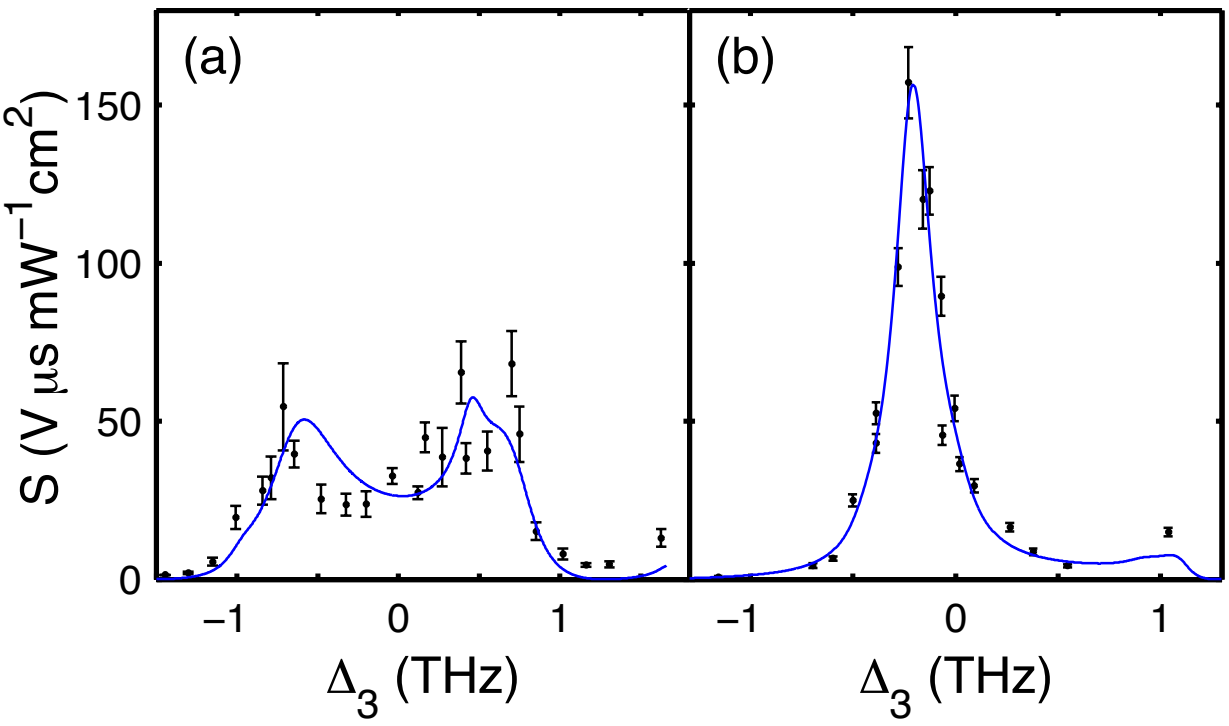

FIG. 3: Autoionization spectra for (a) the 5s19d $^1D_2$ and (b) the 5s20s $^1S_0$ states of strontium. The lines show a fit using a six-channel MQDT model. Δ_3 is the detuning from the $5s_{1/2}$-$5p_{3/2}$ core ion transition (taken from ref[ ]).

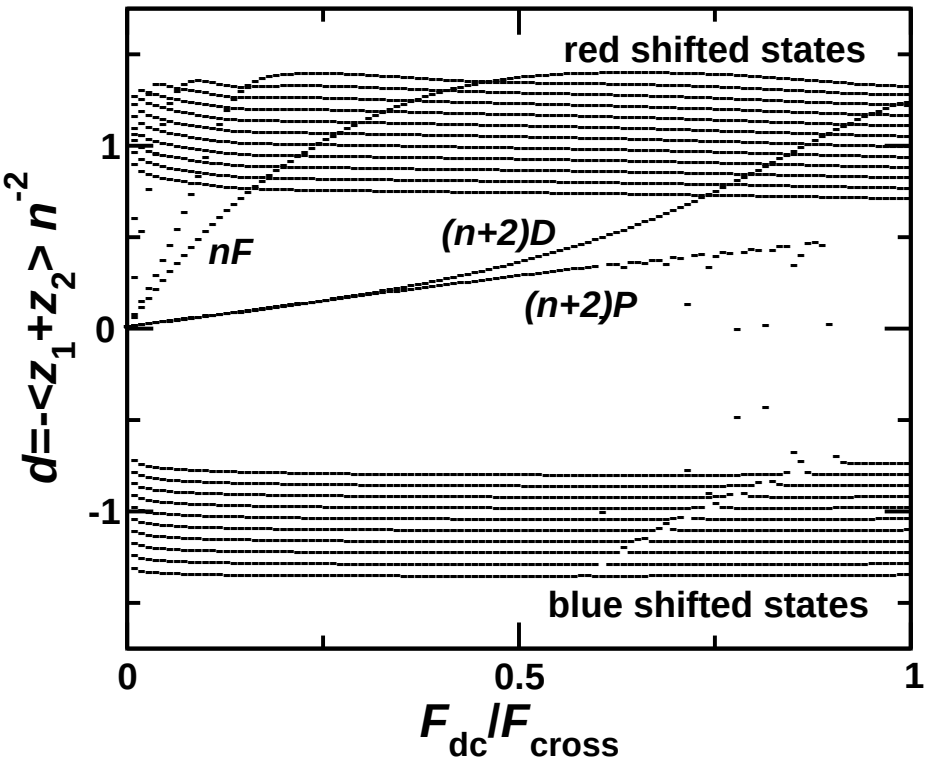

FIG. 4: Calculated scaled dipole moments, d=$\langle z_1 + z_2 \rangle^2/n^2$ for low-L strontium Rydberg states with $n \sim 50$ expressed as a function of applied field normalized to the field, F_{cross}=$1/3n^5$, at which states in neighboring manifolds first cross.

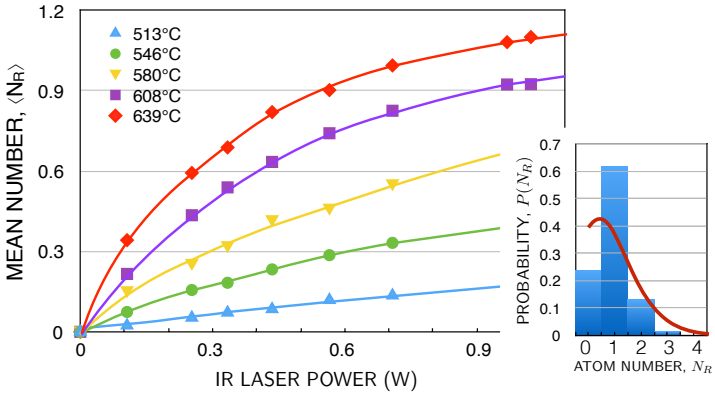

FIG. 5: Mean number, $\langle N_R \rangle$, of n=310 Rydberg atoms excited in a beam during a 130 ns-long laser pulse as a function of 893 nm IR laser power for the oven operating temperatures indicated. The inset shows a typical measured Rydberg number distribution for $\langle N_R \rangle \sim 1$. The line shows a Poissonian distribution for $\langle N_R \rangle = 1$.

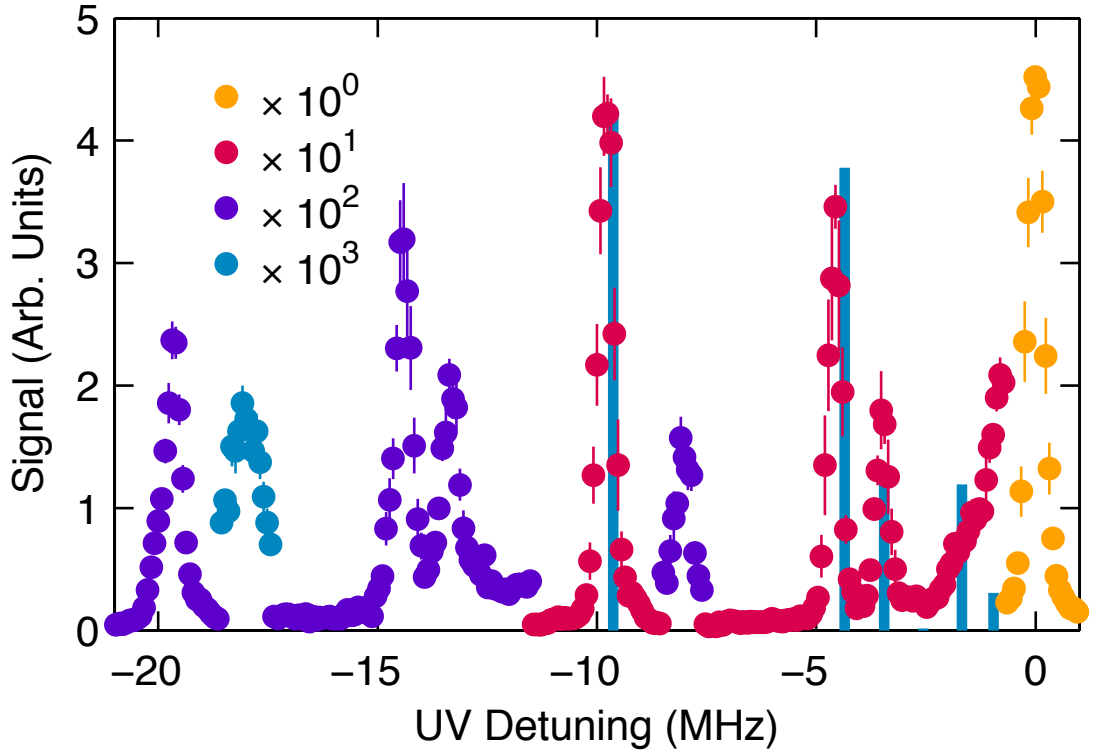

FIG. 6: Rydberg excitation spectrum recorded using a dense cold-gas sample in the vicinity of the strontium 5s38s $^3S_1$ Rydberg state. The calculated positions and relative excitation strengths for the dimer v=0, 1, and 2 vibrational states are indicated by vertical bars. The features at higher binding energies correspond to creation of trimer molecules.

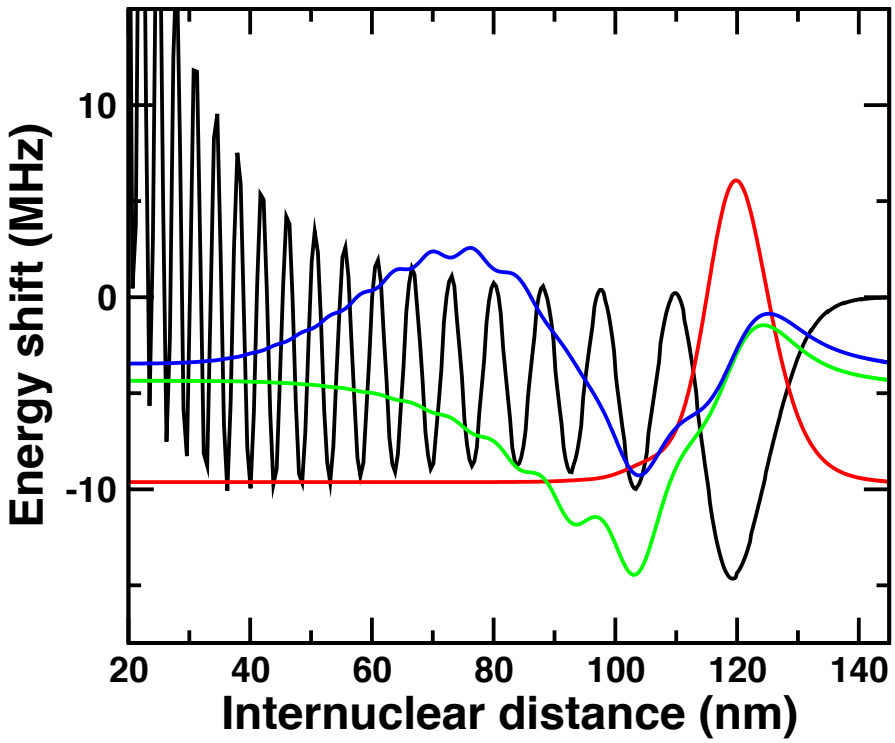

FIG. 7: Calculated molecular potential for a 5s38s $^3S_1$-5s^2 $^1S_0$ strontium atom pair. The colored lines show the calculated wave functions $R\chi_v(R)$ for the v=0, 1, and 2 molecular vibrational states.

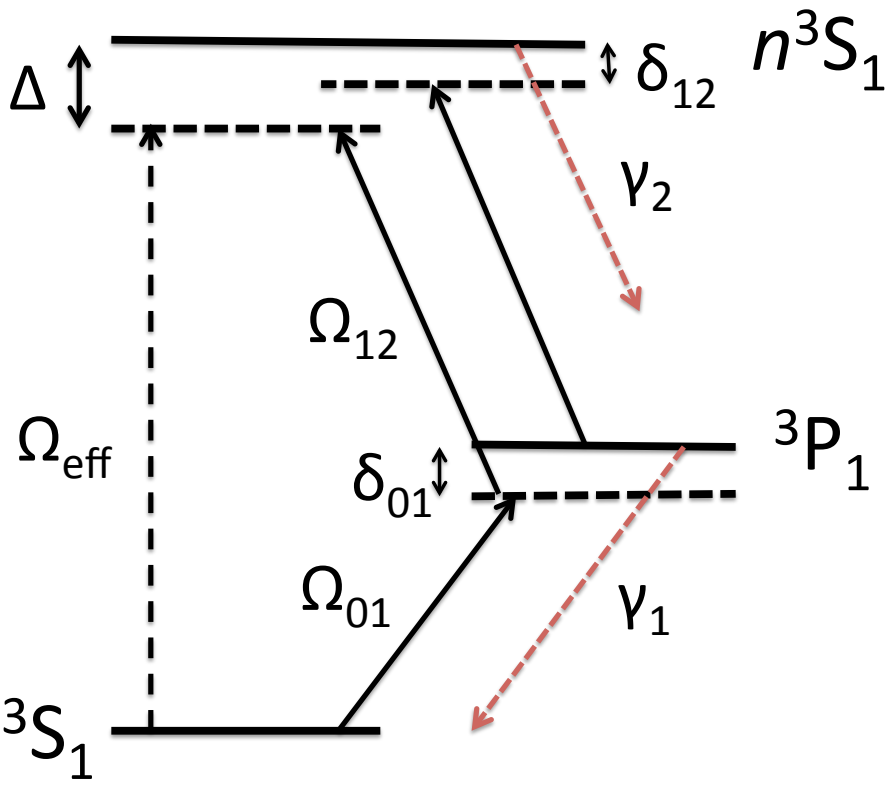

FIG. 8: Schematic diagram of the dressing scheme employed in strontium showing the $^1S_0$ ground state, the intermediate $^3P_1$ state, and the n^3S_1 Rydberg state. The relevant Rabi frequencies Ω_{01} and Ω_{12}, detunings δ_{01}, δ_{12} and Δ , and decay rates γ_1, γ_2 are as indicated.

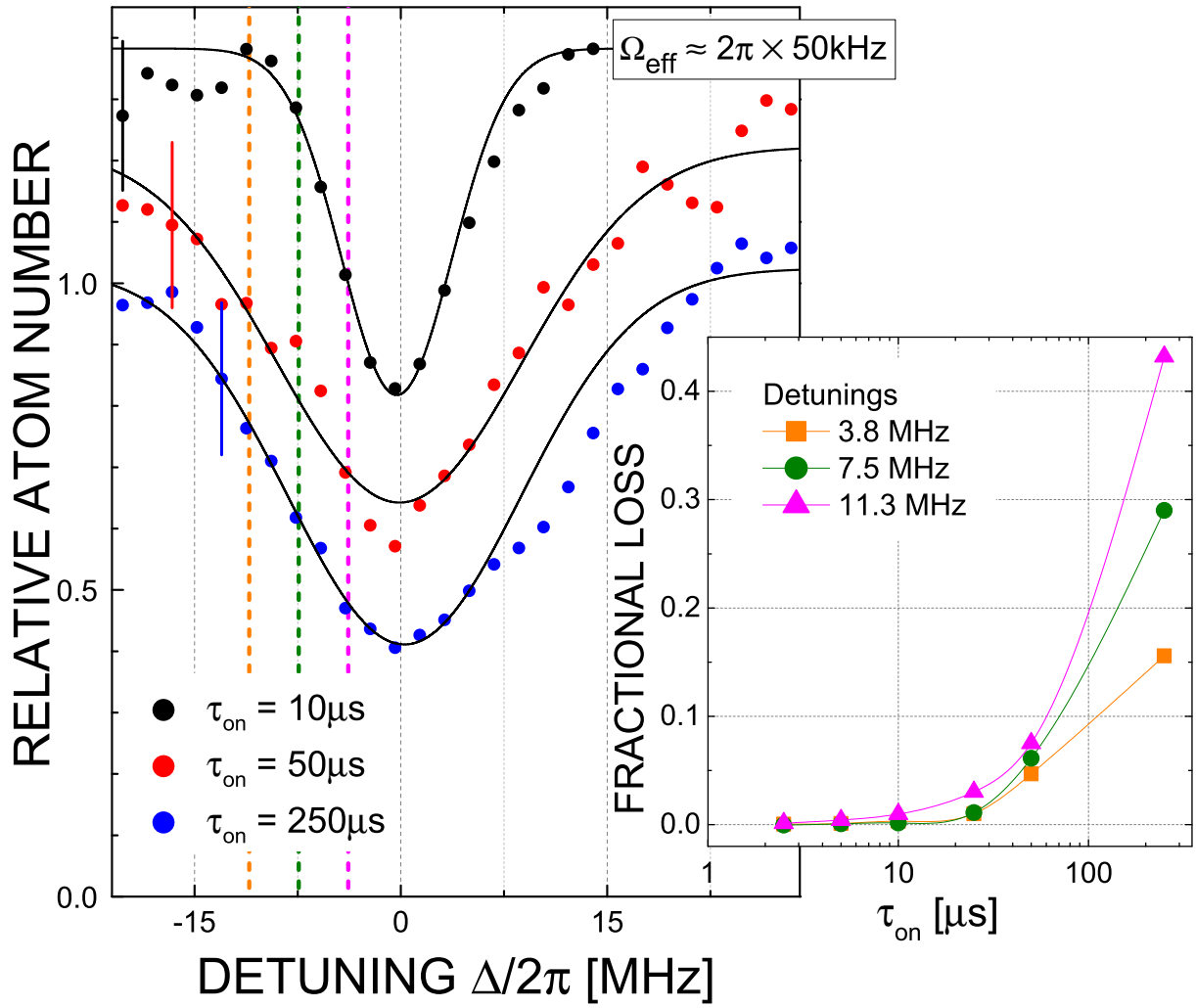

FIG. 9: Measured decrease in the number of ground state atoms present in a ^{84}Sr BEC dressed with the 30^3S_1 Rydberg state and $\Omega_{eff} \sim 2\pi \times 50$ kHz as a function of detuning. Dressing is provided in a series of N pulses, each of equal width t_{on} and separated by100 μs, keeping the total dressing N$\times t_{on}$ constant at 250 μs. The values of t_{on} employed are as indicated. The inset shows the trap loss per pulse for red detunings of ∼3.8, 7.5, and 11.3 MHz as a function of pulse width.

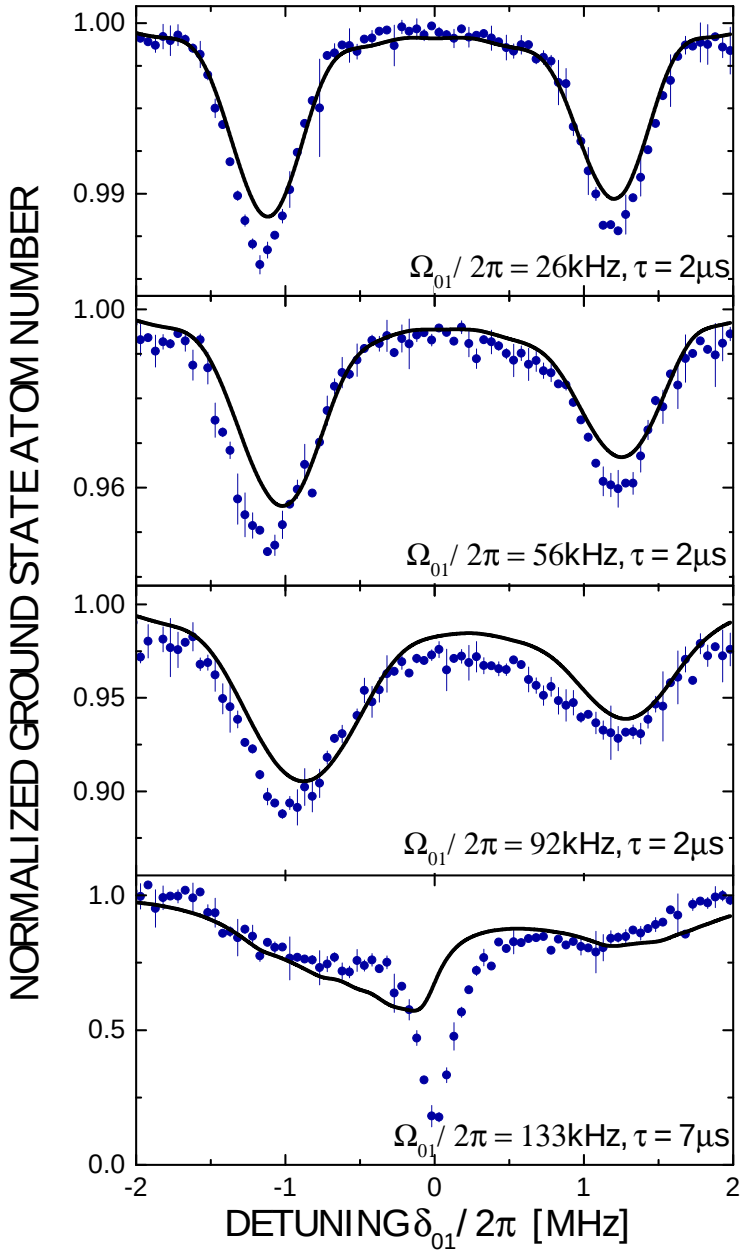

FIG. 10: Fractional number of ground state atoms remaining after a single laser excitation pulse having the widths t_p indicated as a function of detuning δ_{01} for an initial peak density $\sim 1 \times 10^{13}$ cm^{-3} and the values of Ω_{01} indicated (see text). The solid line shows the results of calculations using a density matrix approach accounting for interaction-induced level shifts and dephasing.

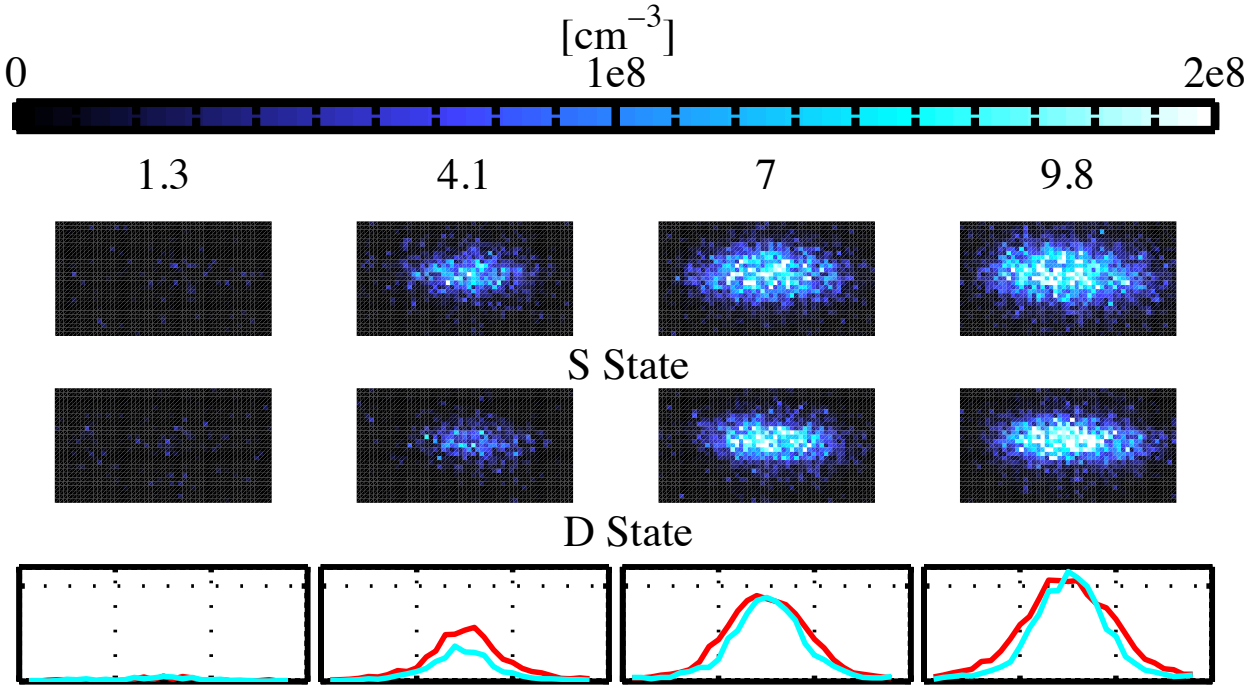

FIG. 11: LIF images showing the spontaneous evolution of the number of visible core ions in an ultracold gas of 48^1S_0 (top) and 47^1D_2 (bottom) Rydberg atoms. The evolution time is indicated above each image and the scale bar represents 1 mm. The initial numbers and densities for both species are identical (see text).